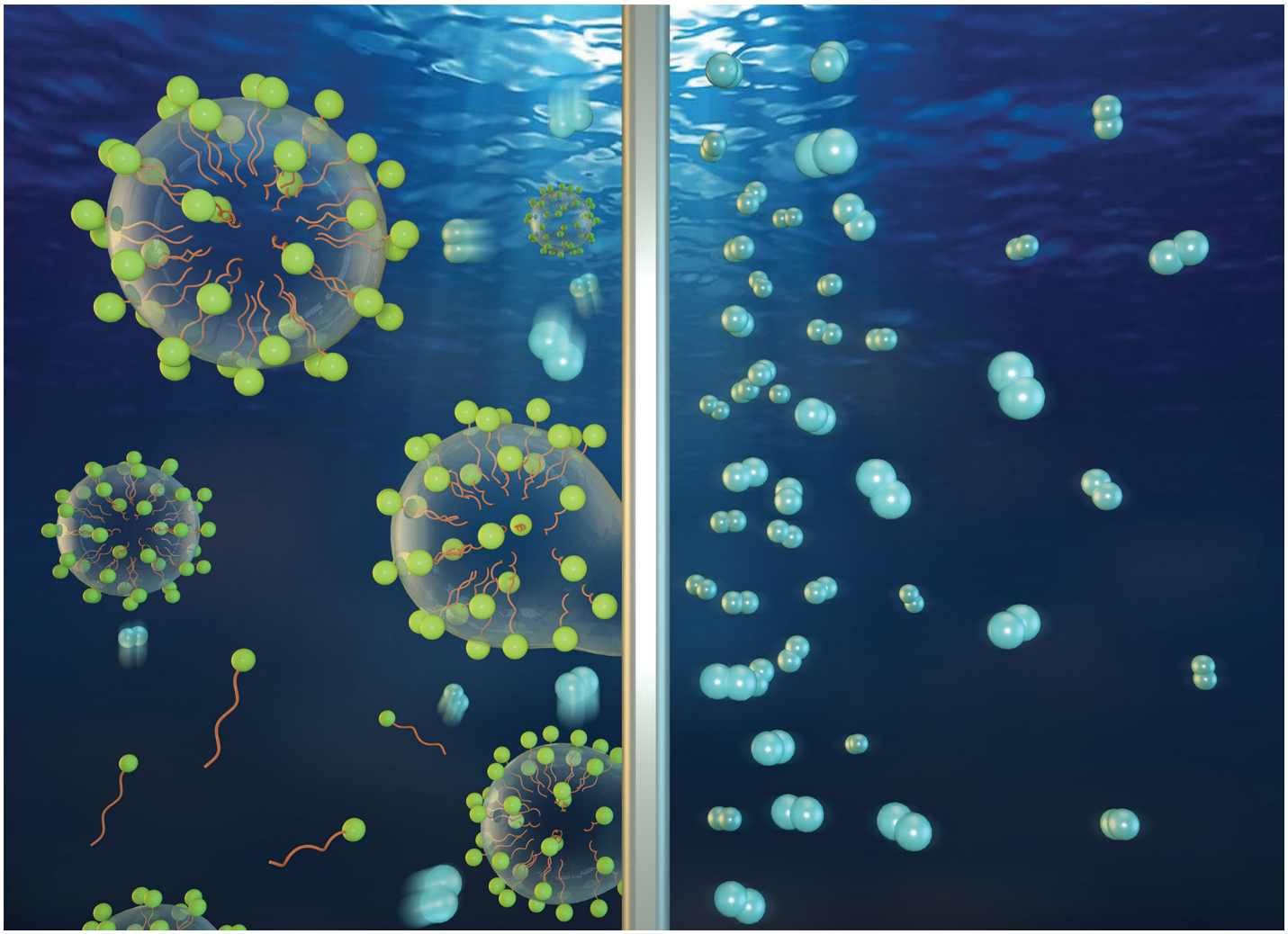

**Showcasing research from Professor Long Luo's laboratory, Department of Chemistry, Wayne State University, Detroit, Michigan, United States.**

Highly efficient hydrogen evolution of platinum *via* tuning the interfacial dissolved-gas concentration

An attractive strategy was demonstrated to manage the interfacial dissolved-gas concentration for the hydrogen evolution reaction. This work provides a comprehensive understanding of gas-involved electrocatalytic process and a rational design of high-performance reaction interface towards the hydrogen evolution reaction.

## As featured in:


See Long Luo *et al.*, *Chem. Commun.*, 2019, **55**, 1378.

ROYAL SOCIETY OF CHEMISTRY | Celebrating IYPT 2019

rsc.li/chemcomm

Registered charity number: 207890

ChemComm

COMMUNICATION

View Article Online
View Journal | View Issue



Cite this: *Chem. Commun.*, 2019, **55**, 1378

Received 5th November 2018,
Accepted 10th December 2018

DOI: 10.1039/c8cc08803a

rsc.li/chemcomm



# Highly efficient hydrogen evolution of platinum *via* tuning the interfacial dissolved-gas concentration†

Xu Zhao, Ruchiranga Ranaweera and Long Luo *

**A facile perfluorooctanesulfonate (PFOS)-modulation strategy was developed to precisely control the dissolved-gas concentration at the electrode/gas/electrolyte interface for enhanced HER. With PFOS modulation, lowered dissolved-hydrogen concentrations at the catalytic interface and sufficient exposure of the surface active area can be achieved. Accordingly, relative to pure Pt, PFOS-modulated Pt possesses a remarkable HER performance.**

Hydrogen is widely regarded as a promising alternative fuel towards a sustainable energy economy owing to its zero carbon footprint and high energy capacity.[1] The hydrogen evolution reaction (HER) has therefore attracted much attention for scalable production of hydrogen with the advantages of high-purity products, accessible reactants and sustainable processes.[2–5] To reduce the overpotential during the HER and achieve a high energy conversion efficiency, tremendous efforts have been made to develop various strategies, such as tuning the adsorption of reaction intermediates on catalysts through manipulating the electronic properties, and maximizing the number of exposed active sites by tailoring the structure of the catalysts.[6–10] For a gas-involved electrocatalytic reaction, the dissolved-gas concentration at the electrode/gas/electrolyte interface, where the catalytic reaction occurs, plays a crucial role in the electrocatalytic performance.[11] Specifically, in a gas-evolving reaction, the overpotential at the interface has been demonstrated to be associated with the concentration of dissolved gas.[12] A low concentration of dissolved hydrogen near the electrode/electrolyte interface can result in a large decrease of overpotential at the interface and thus an elevated hydrogen evolution current.[13] Therefore, it is meaningful and fundamentally important to precisely control the dissolved-gas concentration at the electrode/gas/electrolyte interface for the HER.

Owing to their important role in well-controlled synthesis of structured catalysts, surfactants have been widely employed to modify the morphology, facets and sizes of catalysts through tuning the surface energy.[14–16] For instance, Zeng and co-workers have fabricated cadmium sulfoselenide nanorods with a uniform morphology and size for electrocatalysis using ethylenediamine as the capping surfactant.[17] In addition, platinum-based catalysts with designed nanostructures have been synthesized using sodium dodecylsulfate, hexadecyltrimethylammonium bromide, or oleylamine as the surfactants.[18–21] In particular, these surfactants have a significant impact on the surface tension of the electrolyte solution at the electrode/electrolyte reaction interface,[22] making it a promising approach to manage the electrode/gas/electrolyte interface in gas-involved catalytic reactions.

Herein, by using platinum as the platform, we present a simple and facile strategy to tune the dissolved-gas concentration at the electrode/gas/electrolyte catalytic interface *via* potassium perfluorooctanesulfonate (PFOS) modulation for a dramatically enhanced HER. The addition of PFOS was demonstrated to lower the dissolved-$H_2$ concentration at the reaction interface. Moreover, the desorption of PFOS from the electrode during the HER was monitored to ensure the sufficient exposure of surface active area. Benefiting from the lowered dissolved-gas concentration and sufficient exposure of surface area at the interface, PFOS-modulated Pt exhibited a remarkable electrocatalytic performance towards the HER. Relative to pure Pt, the PFOS-modulated Pt yielded a much lower overpotential of 27 mV at a cathodic current density of 10 mA $cm^{-2}$. Moreover, the PFOS-modulated Pt showed a current density of 26.77 mA $cm^{-2}$ at the overpotential of 0.04 V, which was 2.4-fold higher than that of pure Pt.

To begin with, the Pt nanoelectrode was fabricated *via* a typical electrochemical sharpening process to investigate the reaction process at the electrode/gas/electrolyte interface.[23,24] As shown in Fig. S1 (ESI†), a sharp Pt tip with a radius of curvature of 26 nm was first prepared through electrochemical etching. The as-prepared Pt tip was then sealed in glass and polished with the monitoring of an electronic feedback circuit to obtain the Pt nanoelectrode with an exposed nanodisk. The radius of the Pt nanoelectrode was determined to be 19 nm by the voltammetric steady-state diffusion-limited current for

*Department of Chemistry, Wayne State University, Detroit, Michigan 48202, USA. E-mail: long.luo@wayne.edu*

† Electronic supplementary information (ESI) available: SEM, CV, LSV, Tafel plots, and additional characterization. See DOI: 10.1039/c8cc08803a

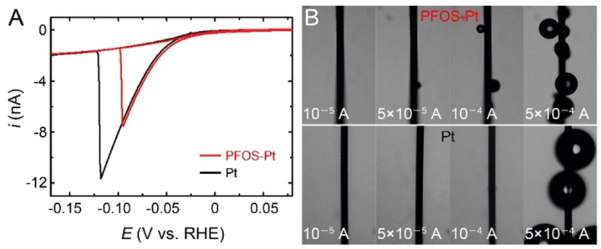


Fig. 1 (A) Typical $i$–$E$ response of Pt nanoelectrodes recorded at a sweep rate of 100 mV $s^{-1}$. (B) *In situ* observation of bubble generation at the interface for PFOS-Pt and pure Pt with different currents.

proton reduction (Fig. S2, ESI†). The generation of a single nanobubble on the Pt nanoelectrode was then monitored using the typical voltammetric method.[25] In comparison, PFOS-modulated Pt, denoted as PFOS-Pt, was measured with the addition of PFOS surfactants at a concentration of $10^{-5}$ mg $mL^{-1}$. As shown in Fig. 1A, with a negative scan of voltage, the current of both the PFOS-Pt and pure Pt nanoelectrodes showed a rapid increase until it reached a peak value ($i_p$), suggesting the formation of a single nanobubble at the surface of the Pt nanoelectrodes.[26] The smooth and continuous $i$–$V$ responses indicated that no bubble formed during this voltage range. Notably, with the addition of PFOS, the PFOS-Pt nanoelectrode exhibited a much lower peak potential than that for the pure Pt nanoelectrode, indicating the facilitated formation of a hydrogen bubble. Meanwhile, the peak current showed an obvious decrease from 11.7 nA to 7.5 nA with PFOS modulation. Given the proportional relationship between the peak current and the critical dissolved-$H_2$ concentration ($C_{H_2}$) needed for bubble formation,[27] which can be described by:

$$i_p = 4nFD_{H_2}C_{H_2}a \quad (1)$$

where $D_{H_2}$ is the diffusivity of $H_2$ and $a$ is the radius of the nanoelectrode, the significantly decreased peak current of PFOS-Pt suggested a much lowered dissolved-$H_2$ supersaturation at the electrode/electrolyte interface, in accordance with the promoted bubble generation. The dissolved-$H_2$ concentration at the interface was as low as 0.11 M for PFOS-Pt. The $H_2$ bubble generation at the reaction interface was further demonstrated by Pt wire electrodes using an optical microscope with a charge-coupled device (CCD). Fig. 1B shows the microscopic images of bubble formation at the surface of PFOS-Pt and pure Pt electrodes. The applied currents for $H_2$ evolution were stepped from $10^{-5}$ A to $5 \times 10^{-4}$ A with a duration time of 10 s at each current step. Obviously, relative to the pure Pt, the PFOS-Pt electrode required a much lower current of $5 \times 10^{-5}$ A for $H_2$ bubble formation, confirming the reduced demand of dissolved-$H_2$ supersaturation and facilitated bubble generation at the reaction interface with PFOS modulation. In addition to the lowered dissolved-$H_2$ supersaturation at the reaction interface, the facilitated bubble formation could lead to a further decrease of dissolved-gas concentration at the reaction interface. The relationship between the overpotential at the interface and the concentration of dissolved gas in a gas-evolving reaction[28] is described by:

$$\eta_c = s_g \frac{RT}{nF} \ln \frac{C_g}{C^{sat}} \quad (2)$$

where $\eta_c$ represents the interfacial overpotential magnitude induced by the dissolved-gas concentration, $C_g$ is the concentration of dissolved gas at the interface, and $C^{sat}$ is the saturation concentration. The largely decreased concentration of dissolved gas at the interface with PFOS modulation can lead to a significantly depressed overpotential, thereby promoting the electrocatalytic HER rate.

As for Pt electrocatalysts, previous mechanistic studies have revealed that the presence of surfactants could hinder the interaction between reaction intermediates and catalytic active sites, and thus have a significant impact on the catalytic performance.[29–32] To gain an in-depth understanding of the behaviours of PFOS surfactants during the HER process, we evaluated the electrochemical active surface areas (ECSAs) of PFOS-Pt during galvanostatic measurement at a cathodic current density of 10 mA $cm^{-2}$. The ECSAs were calculated by collecting the charge in the $H_{upd}$ adsorption/desorption region after double-layer correction (Fig. S3, ESI†) and assuming a value of 210 μC $cm^{-2}$ for the adsorption of a monolayer of hydrogen on the Pt surface.[33] Before the galvanostatic test, PFOS-Pt showed an initial ECSA of 0.117 $cm^2$, smaller than that of 0.155 $cm^2$ for pure Pt, indicating the partial blockage of surface active sites by PFOS addition. However, after the galvanostatic measurement for 40 s at 10 mA $cm^{-2}$, the PFOS-Pt exhibited an increase of 10.6% in ECSA (Fig. 2A). Such an increase in ECSA for PFOS-Pt indicated the efficient desorption of PFOS surfactants from the surface of the Pt electrode during the HER process. The desorption of PFOS could be attributed to the electrostatic interaction between the anionic surfactants and the negatively charged Pt surface.[34,35] In contrast, without the PFOS modulation, the pure Pt showed a decrease of 6.7% in ECSA after 40 s, which is mainly derived from the dramatic damage of the electrode structure during the continuous HER,[36] further suggesting the desorption of PFOS for the PFOS-Pt electrode. To further investigate the PFOS behaviours on the Pt electrodes, the ECSAs of PFOS-Pt with different galvanostatic reaction times were measured (Fig. 2B). With the increase of catalytic reaction time, the ECSAs of PFOS-Pt showed a similar decreasing trend to that of the pure Pt electrode. In particular, after the galvanostatic reaction for 160 s, the ECSA of PFOS-Pt was 0.091 $cm^2$, consistent with the ECSA of 0.093 $cm^2$ for pure Pt, further demonstrating the desorption of PFOS from the surface of the Pt electrode. Moreover, relative to pure Pt, the normalized ECSAs for PFOS-Pt showed a similar decreasing trend and larger values after the long-term galvanostatic test (Fig. S4, ESI†), further suggesting the desorption of PFOS. As such, the desorption of PFOS from the

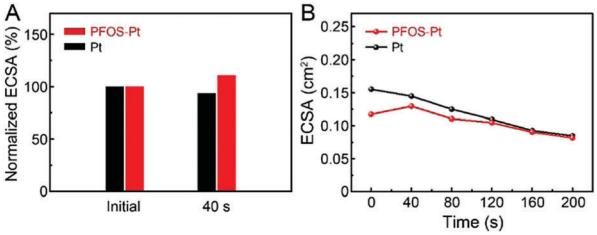


Fig. 2 (A) Comparison of normalized ECSA for PFOS-Pt and pure Pt after the galvanostatic test for 40 s at 10 mA $cm^{-2}$. (B) ECSA of PFOS-Pt and Pt before and after the long-term galvanostatic test.

Pt surface during catalytic processes can ensure sufficient exposure of surface active areas, leading to an efficient HER.

The electrocatalytic HER properties of PFOS-Pt were further evaluated in a $N_2$-saturated 0.5 M $HClO_4$ solution in comparison with pure Pt. Fig. 3A shows the typical polarization curves recorded *via* linear sweep voltammetry (LSV) at a slow sweep rate of 2 mV $s^{-1}$ and a rotating speed of 1600 rpm. The rotating speed was applied during the test to remove the generated bubbles (Fig. S5, ESI†). The ohmic potential drop (iR) losses from the electrolyte were all corrected before comparison. Notably, PFOS-Pt exhibited a remarkable performance with a much earlier HER onset potential and higher current densities than those of pure Pt. At the cathodic current density of 10 mA $cm^{-2}$, which represents a metric related to the solar fuel conversion,[37] the overpotential of PFOS-Pt was only 27 mV, much lower than that of pure Pt (38 mV). Moreover, the inset shows the cathodic current densities at the overpotential of 0.04 V, making it available to directly compare the electrocatalytic activities. The PFOS-Pt presented a cathodic current density of 26.77 mA $cm^{-2}$, which was 2.4 times as high as that of pure Pt, suggesting the much enhanced HER performance with PFOS modulation. Furthermore, the corresponding Tafel plots were evaluated to gain in-depth insight into the hydrogen evolution activity. As shown in Fig. 3B, PFOS-Pt possesses a relatively smaller Tafel slope of 26 mV $dec^{-1}$ than that for pure Pt (32 mV $dec^{-1}$), demonstrating the accelerated HER kinetics. The results indicated that the HER process occurred following a Volmer–Tafel mechanism, in which the recombination of adsorbed H species acts as the rate-determining reaction.[38] The small Tafel slope induced by PFOS modulation could drive a large catalytic current at low overpotential, which is in accordance with the elevated activities shown by polarization curves and beneficial for practical applications. The activity enhancement was also observed using Pt mesh and Au with PFOS modulation (Fig. S6, ESI†). In addition, the durability tests under a constant cathodic current density of 10 mA $cm^{-2}$ indicate that PFOS-Pt possesses better durability than pure Pt (Fig. S7, ESI†). Taken together, the enhancement of the catalytic performance for PFOS-Pt could be attributed to the following factors: (i) lowered dissolved-$H_2$ concentration at the electrode/electrolyte interface due to the PFOS modulation, and (ii) sufficient exposure of the surface active area due to the efficient desorption of surfactants, leading to a remarkably promoted HER rate.

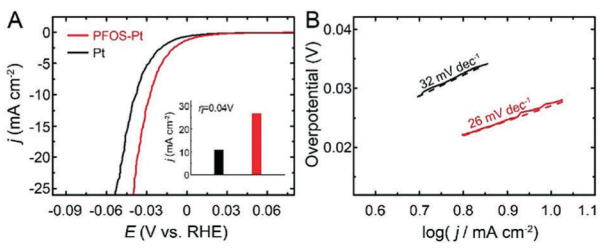


Fig. 3 (A) iR-corrected polarization curves of PFOS-Pt and pure Pt in $N_2$-saturated 0.5 M $HClO_4$ solution. The inset shows the current densities of PFOS-Pt and pure Pt at the overpotential of 0.04 V. (B) Tafel plots of PFOS-Pt and pure Pt.

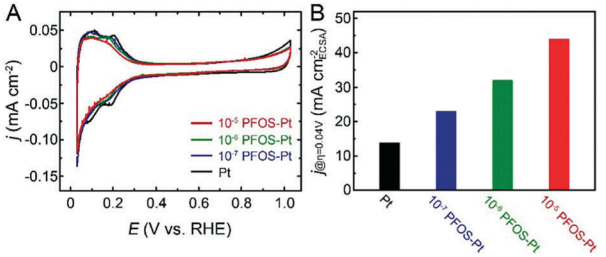


Fig. 4 (A) CV curves of PFOS-Pt with different PFOS concentrations recorded at a sweep rate of 50 mV $s^{-1}$. (B) HER specific activities of PFOS-Pt normalized by ECSA.

In addition, to further investigate the concentration-dependent HER performance, PFOS-Pt with different PFOS concentrations ($10^{-7}$, $10^{-6}$, and $10^{-5}$ mg $mL^{-1}$) was also measured. Fig. 4A shows the typical CVs obtained in a $N_2$-saturated 0.5 M $HClO_4$ solution at a scan rate of 50 mV $s^{-1}$. Notably, with the increase of PFOS concentration, the ECSAs, which were calculated from the $H_{upd}$ adsorption/desorption regions, exhibited a decrease. The corresponding HER activities of PFOS-Pt increased monotonically, with PFOS concentrations rising from $10^{-7}$ mg $mL^{-1}$ to $10^{-5}$ mg $mL^{-1}$ (Fig. S8, ESI†). In particular, PFOS-Pt with the PFOS concentration of $10^{-5}$ mg $mL^{-1}$ displayed the smallest overpotential and lowest Tafel slopes among all the tested electrodes. The $10^{-5}$ PFOS-Pt also showed a better activity than those with PFOS concentrations higher than $10^{-5}$ mg $mL^{-1}$ (Fig. S9, ESI†). To better understand the surface effects, the specific activities of PFOS-Pt were compared through normalizing the currents by active surface area. As illustrated in Fig. 4B, $10^{-5}$ PFOS-Pt exhibited a cathodic current density of 43.96 mA $cm^{-2}_{ECSA}$ at the fixed overpotential of 0.04 V, which was 1.4, 1.9 and 3.2 times as high as that of $10^{-6}$ PFOS-Pt, $10^{-7}$ PFOS-Pt and pure Pt. In view of the 16.9% variation in ECSA during the HER (Fig. S10, ESI†), the significantly increased current density for $10^{-5}$ PFOS-Pt further demonstrated the largely boosted intrinsic activity.

In summary, we develop an ingenious PFOS-modulation strategy with precisely managed dissolved-gas concentration at the electrode/gas/electrolyte interface for highly efficient hydrogen evolution. With the modulation of PFOS, facilitated bubble generation and decreased dissolved-gas concentration at the reaction interface can be achieved. Meanwhile, the desorption of PFOS for the sufficient exposure of surface active area of the electrode was also monitored during the HER, leading to a remarkably improved HER performance. This work provides a systematic understanding of the gas-involved catalytic process at the electrode/gas/electrolyte interface and a convenient approach to realizing high-performance electrocatalysis based on precisely controlling the dissolved-gas concentration at the catalytic interface.

This work was supported by the start-up funds and the Ebbing Faculty Development Award from Wayne State University.

## Conflicts of interest

There are no conflicts to declare.

 

## Notes and references

1 Y. M. Shi and B. Zhang, *Chem. Soc. Rev.*, 2016, **45**, 1529.
2 G. B. Chen, T. Wang, J. Zhang, P. Liu, H. J. Sun, X. D. Zhuang, M. W. Chen and X. L. Feng, *Adv. Mater.*, 2018, **30**, 1706279.
3 S. Hao, L. B. Yang, D. N. Liu, R. M. Kong, G. Du, A. M. Asiri, Y. C. Yang and X. P. Sun, *Chem. Commun.*, 2017, **53**, 5710.
4 J. X. Feng, J. Q. Wu, Y. X. Tong and G. R. Li, *J. Am. Chem. Soc.*, 2018, **140**, 610.
5 S. L. Zhou, X. H. Chen, P. Yu, F. Gao and L. Q. Mao, *Electrochem. Commun.*, 2018, **90**, 91.
6 R. He, J. Hua, A. Q. Zhang, C. H. Wang, J. Y. Peng, W. J. Chen and J. Zeng, *Nano Lett.*, 2017, **17**, 4311.
7 Y. W. Liu, X. M. Hua, C. Xiao, T. F. Zhou, P. C. Huang, Z. P. Guo, B. C. Pan and Y. Xie, *J. Am. Chem. Soc.*, 2016, **138**, 5087.
8 M. R. Gao, Y. R. Zheng, J. Jiang and S. H. Yu, *Acc. Chem. Res.*, 2017, **50**, 2194.
9 Z. W. Seh, J. Kibsgaard, C. F. Dickens, I. Chorkendorff, J. K. Norskov and T. F. Jaramillo, *Science*, 2017, **355**, eaad4998.
10 C. Meng, T. Ling, T. Y. Ma, H. Wang, Z. P. Hu, Y. Zhou, J. Mao, X. W. Du, M. Jaroniec and S. Z. Qiao, *Adv. Mater.*, 2017, **29**, 1604607.
11 M. Liu, Y. J. Pang, B. Zhang, P. D. Luna, O. Voznyy, J. X. Xu, X. L. Zheng, C. T. Dinh, F. J. Fan, C. H. Cao, F. P. G. Arquer, T. S. Safaei, A. Mepham, A. Klinkova, E. Kumacheva, T. Filleter, D. Sinton, S. O. Kelley and E. H. Sargent, *Nature*, 2016, **537**, 382.
12 H. Vogt, *J. Electrochem. Soc.*, 1990, **137**, 1179.
13 J. Dukovic and C. W. Tobias, *J. Electrochem. Soc.*, 1987, **134**, 331.
14 Y. N. Xia, Y. J. Xiong, B. Lim and S. E. Skrabalak, *Angew. Chem., Int. Ed.*, 2009, **48**, 60.
15 R. Long, S. Zhou, B. J. Wiley and Y. J. Xiong, *Chem. Soc. Rev.*, 2014, **43**, 6288.
16 Z. X. Fan and H. Zhang, *Chem. Soc. Rev.*, 2016, **45**, 63.
17 R. He, A. Zhang, Y. L. Ding, T. Y. Kong, Q. Xiao, H. L. Li, Y. Liu and J. Zeng, *Adv. Mater.*, 2018, **30**, 1705872.
18 Z. M. Peng and H. Yang, *Nano Today*, 2009, **4**, 143.
19 J. J. Mao, W. X. Chen, D. S. He, J. W. Wan, J. J. Pei, J. C. Dong, Y. Wang, P. F. An, Z. Jin, W. Xing, H. L. Tang, Z. B. Zhuang, X. Liang, Y. Huang, G. Zhou, L. Y. Wang, D. S. Wang and Y. D. Li, *Sci. Adv.*, 2017, **3**, e1603068.
20 Q. Li, L. H. Wu, G. Wu, D. Su, H. F. Lv, S. Zhang, W. L. Zhu, A. Casimir, H. Y. Zhu, A. M. Garcia and S. H. Sun, *Nano Lett.*, 2015, **15**, 2468.
21 V. Beermann, M. Gocyla, S. Kuhl, E. Padgett, H. Schmies, M. Goerlin, N. Erini, M. Shviro, M. Heggen, R. E. D. Borkowski, D. A. Muller and P. Strasser, *J. Am. Chem. Soc.*, 2017, **139**, 16536.
22 C. Frese, S. Ruppert, M. Sugar, H. S. Lewerkuhne, K. P. Wittern, V. B. Fainerman, R. Eggers and R. Miller, *J. Colloid Interface Sci.*, 2003, **267**, 475.
23 B. Zhang, J. Galusha, P. G. Shiozawa, G. L. Wang, A. J. Bergren, R. M. Jones, R. J. White, E. N. Ervin, C. C. Cauley and H. S. White, *Anal. Chem.*, 2007, **79**, 4778.
24 Y. L. Ying, Z. F. Ding, D. P. Zhan and Y. T. Long, *Chem. Sci.*, 2017, **8**, 3338.
25 H. Ren, S. R. German, M. A. Edwards, Q. J. Chen and H. S. White, *J. Phys. Chem. Lett.*, 2017, **8**, 2450.
26 Q. J. Chen and L. Luo, *Langmuir*, 2018, **34**, 4554.
27 Q. J. Chen, H. S. Wiedenroth, S. R. German and H. S. White, *J. Am. Chem. Soc.*, 2015, **137**, 12064.
28 C. Gabrielli, F. Huet and R. P. Nogueira, *Electrochim. Acta*, 2005, **50**, 3726.
29 D. G. Li, C. Wang, D. Tripkovic, S. H. Sun, N. M. Markovic and V. R. Stamenkovic, *ACS Catal.*, 2012, **2**, 1358.
30 M. Cargnello, C. Chen, B. T. Diroll, V. V. T. D. Nguyen, R. J. Gorte and C. B. Murray, *J. Am. Chem. Soc.*, 2015, **137**, 6906.
31 H. J. Yin, H. J. Tang, D. Wang, Y. Gao and Z. Y. Tang, *ACS Nano*, 2012, **6**, 8288.
32 C. L. Zhang, S. N. Oliaee, S. Y. Hwang, X. K. Kong and Z. M. Peng, *Nano Lett.*, 2016, **16**, 164.
33 A. Guha, T. V. Vineesh, A. Sekar, S. Narayanaru, M. Sahoo, S. Nayak, S. Chakraborty and T. N. Narayanan, *ACS Catal.*, 2018, **8**, 6636.
34 N. Liu, Q. D. Zhang, R. X. Qu, W. F. Zhang, H. F. Li, Y. Wei and L. Feng, *Langmuir*, 2017, **33**, 7380.
35 C. S. Cha and Y. B. Zu, *Langmuir*, 1998, **14**, 6280.
36 Y. J. Li, H. C. Zhang, T. H. Xu, Z. Y. Lu, X. C. Wu, P. B. Wan, X. M. Sun and L. Jiang, *Adv. Funct. Mater.*, 2015, **25**, 1737.
37 C. C. L. McCrory, S. Jung, I. M. Ferrer, S. M. Chatman, J. C. Peters and T. F. Jaramillo, *J. Am. Chem. Soc.*, 2015, **137**, 4347.
38 G. R. Xu, J. Bai, L. Yao, Q. Xue, J. X. Jiang, J. H. Zeng, Y. Chen and J. M. Lee, *ACS Catal.*, 2017, **7**, 452.